Nanomagnetic Droplets and Implications to Orbital Ordering in $La_{1-x}Sr_xCoO_3$

D. Phelan,[1] Despina Louca,[1,*] S. Rosenkranz,[2] S.-H. Lee,[1] Y. Qiu,[3,4] P. J. Chupas,[2] R. Osborn,[2] H. Zheng,[2] J. F. Mitchell,[2] J. R. D. Copley,[3] J. L. Sarrao,[5] and Y. Moritomo[6]

[1]*Department of Physics, University of Virginia, Charlottesville, Virginia 22904, USA*
[2]*Materials Science Division, Argonne National Laboratory, Argonne, Illinois 60439, USA*
[3]*NIST Center for Neutron Research, Gaithersburg, Maryland 20899, USA*
[4]*Department of Materials Science and Engineering, University of Maryland, College Park, Maryland 20742, USA*
[5]*Los Alamos National Laboratory, Los Alamos, New Mexico 87545, USA*
[6]*Department of Applied Physics, Nagoya University, Nagoya 464-8603, Japan*

(Received 23 May 2005; published 17 January 2006)

Inelastic cold-neutron scattering on $LaCoO_3$ provided evidence for a distinct low energy excitation at 0.6 meV coincident with the thermally induced magnetic transition. Coexisting strong ferromagnetic (FM) and weaker antiferromagnetic correlations that are *dynamic* follow the activation to the excited state, identified as the intermediate $S = 1$ spin triplet. This is indicative of dynamical orbital ordering favoring the observed magnetic interactions. With hole doping as in $La_{1-x}Sr_xCoO_3$, the FM correlations between Co spins become static and isotropically distributed due to the formation of FM droplets. The correlation length and condensation temperature of these droplets increase rapidly with metallicity due to the double exchange mechanism.

DOI: 10.1103/PhysRevLett.96.027201 PACS numbers: 75.40.Gb, 61.12.−q, 71.30.+h, 71.70.−d

Transition metal oxides display rich phase diagrams due to strong correlation effects resulting from competing crystal field, spin-spin, and spin-orbit interactions. The rhombohedral perovskite $LaCoO_3$ with $R\bar{3}c$ symmetry is a prime example where by manipulating the magnetic exchange and electron-phonon couplings either thermally or with doping [1–3], unconventional transport and magnetic characteristics emerge [4]. The ground state of the octahedrally coordinated Co^{3+} ion is the nonmagnetic $S = 0$ that corresponds to the low spin, $t_{2g}^6 e_g^0$ configuration. As the gap (Δ) between the t_{2g} and e_g orbital states becomes small in the presence of a large trigonal distortion [1,5] aided by strong Co-O hybridization [6], the system can be thermally excited to a magnetic state. Evidence for this is provided by a broad peak in the bulk susceptibility, χ, [1,7–9] ~100 K that marks the onset to a paramagnetic (PM) state. The excited state can either be the so-called $S = 1$ intermediate spin (IS) state with a $t_{2g}^5 e_g^1$ configuration or the $S = 2$ high spin (HS) state with a $t_{2g}^4 e_g^2$ configuration. The two states are fundamentally distinct and should lead to very different interactions, considering that the $S = 1$ state is accompanied by orbital degeneracy and is Jahn-Teller active while the $S = 2$ state is not. The low temperature dependence of χ has been fit equally well with models that consider either spin state [8,10] making this a controversial issue for several decades [7–9,11]. Identifying the excited state that leads to the magnetic transition is important as it provides insight into the nature of the Co^{3+} ion interactions. Early thermal neutron scattering measurements showed the existence of dynamic ferromagnetic (FM) correlations [11] but the absence of studies on the low energy excitations has hindered the critical understanding of the transition mechanism and is the focus of the present work.

The interactions become even more complex with the introduction of charge carriers and the mixing of Co^{3+} with Co^{4+} ions [9]. When holes are doped by replacing the trivalent La^{3+} ions with divalent Sr^{2+} ions in $La_{1-x}Sr_xCoO_3$, a spin glass ($x > 5\%$) and a FM-metallic (FMM) state ($x > 18\%$) emerge in the phase diagram but without a structural transition as in the isostructural colossal magnetoresistive manganites. Reports on the characteristic dynamics and spatial extent of the magnetic correlations provided limited information. Using the nuclear magnetic resonance (NMR) technique that probes local slow dynamics it was shown that the magnetic correlations develop to an FM cluster glass with doping [12]. A more recent NMR study suggested coexistence of FM and non-FM components [13] proposed to be driven by tendencies for phase separation, resulting in an inhomogeneous metallic state. In this Letter, we focus on the spatial distribution of the FM correlations and probe both their dynamic and static characteristics. Our results suggest that the intimate relation of the magnetic exchange energy to the orbital ordering tendency and electronic configuration is key to understanding the physical nature of the undoped $LaCoO_3$ as well as of the $La_{1-x}Sr_xCoO_3$.

Using cold-neutron elastic and inelastic scattering with high instrumental resolution, we investigated the kind of spin correlations in $La_{1-x}Sr_xCoO_3$, with $x = 0.0$, 0.10, 0.15, and 0.20, that prevails in the nonmagnetic insulating through the spin glass to the FMM state. In undoped $LaCoO_3$, a distinct low energy excitation peak at ~0.6 meV was observed in support of the thermal activation of a zero-field split $S = 1$ spin state. Concomitant with the population of this magnetic state are strong dynamic short-range FM *and* weaker antiferromagnetic (AFM) correlations observed for the first time that in turn provide

evidence for dynamic orbital ordering conducive to the observed magnetic interactions. Upon doping, the short-range FM correlations become static while the dynamic AFM correlations disappear. Direct evidence for isotropic spread of the FM correlations indicating the formation of FM droplets is provided. The size of these FM droplets and their correlation length increase gradually at first in the spin glass phase and more rapidly in the FM metallic phase. Through the double exchange (DE) mechanism, the orbital states of Co^{4+} and Co^{3+} within the droplets allow for charges to propagate throughout the crystal structure.

Polycrystalline samples of $LaCoO_3$ (30 g) and single crystals of $La_{1-x}Sr_xCoO_3$ with $x = 0.0$, 0.10, 0.15, and 0.20 (grown using the floating zone technique and ~6 g each) were used for the elastic and inelastic measurements. The powder samples were studied using the cold-neutron time-of-flight Disk Chopper Spectrometer (DCS) [14] at the NIST Center for Neutron Research (NCNR) with an incident wavelength of 5.0 Å (equivalent to an incident energy E_i of 3.27 meV). The single crystals were measured using the cold-neutron triple-axis spectrometer SPINS at the NCNR, with a fixed final energy of $E_f = 3.7$ meV. The instrumental energy resolution was $\Delta E = 0.22$ meV. The single crystals were mounted in the (h, h, l) scattering plane using the pseudocubic notation and a room temperature lattice constant $a = 3.8377$ Å. A cooled BeO filter was placed in the scattered beam to eliminate higher order contaminations.

$LaCoO_3$ was measured using the DCS spectrometer at temperatures ranging from 10 to 300 K. As this system is not magnetic at low temperatures, the 10 K data were used as the background and subtracted from data at the other temperatures to obtain the dynamical structure factor, $S(Q, \hbar\omega)$, where Q is the momentum transfer and $\hbar\omega$ is the energy. The $S(Q, \hbar\omega)$ was normalized in absolute units with an accuracy of 20% by comparison with the nuclear Bragg intensities [15]. The $S(\hbar\omega)$ shown in Fig. 1 was obtained by integrating from $Q = 0.5$ to 2.0 $Å^{-1}$. Near $\hbar\omega = 0$, the data appear noisy because the low temperature elastic peak is subtracted from the higher temperature data. No observable signal is evident in the data beyond the elastic region at the first temperature shown, 25 K, indicating that the system is still nonmagnetic at this temperature [Fig. 1(a)]. With increasing temperature, the intensity increases at low energies and consists of two components: a broad inelastic continuum centered at $\hbar\omega = 0$ and distinct excitations at ± 0.6 meV [16]. The low energy inelastic scattering is commonly seen in paramagnetic phases of magnetic systems, and it continues to grow up to about 100 K. The peaks at ± 0.6 meV first increase in intensity and become well defined by 50 K [Fig. 1(b)] but then seem to fade away above 75 K [Figs. 1(c) and 1(d)]. The fading is, however, a consequence of the powder average and is not seen in the single crystal data discussed below. The

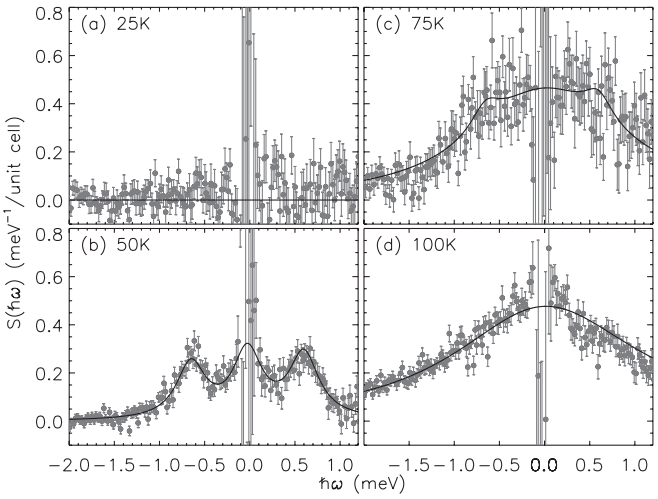

FIG. 1. The $\hbar\omega$ dependence of the neutron scattering cross section, $S(\hbar\omega)$, obtained from the DCS measurements on a powder sample of $LaCoO_3$ at various temperatures: (a) 25, (b) 50, (c) 75, and (d) 100 K.

solid lines in the figure are the fits to $S(\hbar\omega) = \frac{\chi''(\hbar\omega)}{\pi(1-e^{-\beta\hbar\omega})}$ where the imaginary susceptibility $\chi''(\hbar\omega)$ [18] is given by two Lorentzian functions to account for the energy width of the two components:

$$\chi''(\hbar\omega) = \frac{\chi_0\Gamma_0\omega}{\omega^2 + \Gamma_0^2} + \frac{\chi_1\Gamma_1|\omega \pm \omega_0|}{(\omega \pm \omega_0)^2 + \Gamma_1^2}. \qquad (1)$$

ω_0 was fixed at 0.625 meV, Γ_0 and Γ_1 (with Γ_1 fixed at 0.197 meV) are the relaxation rates, and χ_1 is the amplitude of the 0.6 meV excitations. The first term corresponding to the inelastic continuum intensity contains χ_0, the static staggered susceptibility, is compared to the bulk susceptibility, χ (Fig. 2). The almost identical temperature dependence of χ_0 to χ clearly indicates the magnetic origin

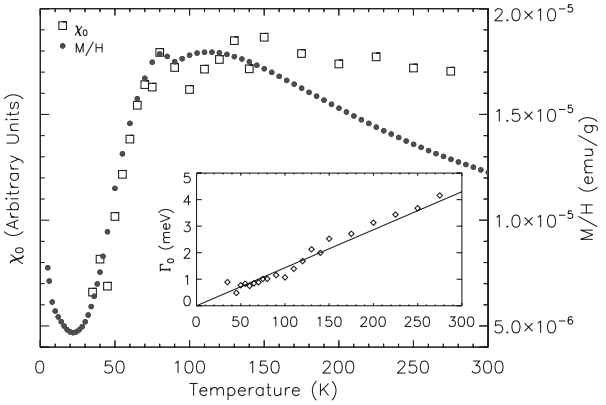

FIG. 2. The temperature dependence of the static staggered susceptibility, χ_0, as determined from Eq. (1) (open squares) and the bulk magnetic susceptibility, χ (solid circles). The upturn below 35 K in χ might be from a surface ferromagnetic component as described in Ref. [25]. Beyond 75 K, the two peaks are not resolved and only one term is used for fitting $\chi''(\hbar\omega)$.

of the two. Shown in the inset is Γ_0 that behaves linearly with temperature, $\Gamma_0 = 0.0143 k_B T$.

The single crystal results on $LaCoO_3$ as a function of $\hbar\omega$ and $\vec{Q}$ carried out at SPINS are summarized in Fig. 3. The constant-$\vec{Q}$ scans in Figs. 3(a) and 3(b) performed around the FM $\vec{Q} = (001)$ and AFM $\vec{Q} = (\frac{1}{2}, \frac{1}{2}, 0)$ wave vectors show that the 0.6 meV mode is clearly present at temperatures higher than 75 K, in contrast to the powder data of Fig. 1. Also shown are constant $\hbar\omega = 0.6$ meV scans around $\vec{Q} = (001)$ and $\vec{Q} = (\frac{1}{2}, \frac{1}{2}, \frac{1}{2})$ in Figs. 3(c) and 3(d) from which the magnetic scattering is separated to three distinct components: dynamic AFM and FM correlations as well as single-ion contributions that provide the $\vec{Q}$-independent constant term underneath the FM and AFM peaks. While the latter shows little or no temperature dependence, the AFM and FM correlations change considerably with temperature. At 55 K, a distinct peak is present at the FM point $\vec{Q} = (001)$ [Fig. 3(c)], whereas at the AFM point $\vec{Q} = (\frac{1}{2}, \frac{1}{2}, \frac{1}{2})$ only the single-ion contributions are visible. At 100 K, the FM peak gains in intensity while a clear peak appears at the AFM point as well with about half of the intensity of the FM peak. We will argue below that the 0.6 meV peak arises from single-ion transitions within the $S = 1$ triplet manifold.

Upon doping with 10% Sr, the 0.6 meV mode disappears as shown for data collected at 100 K for a scan performed around the FM $\vec{Q} = (001)$ point [Fig. 3(b)]. Also at this temperature, FM dynamic fluctuations are still present but suppressed, while the AFM ones are absent altogether [Figs. 3(c) and 3(d)]. The PM fluctuations although suppressed are also present. With cooling, the $x = 0.10$ sample starts to exhibit static short-range FM ordering below 70 K, as shown in Figs. 4(a) and 4(b). The elastic FM peak becomes sharp and strong, whereas the PM fluctuations weaken as the Sr concentration increases corresponding to the enhancement of static FM correlations. The elastic neutron scattering mapped in the vicinity of the (001) point in the (hhl) scattering plane shows that the spatial extent of the FM correlations is isotropic for all values of x shown. The enhancement of ferromagnetism with increasing x is also reflected in the spin freezing temperature, T_c, defined as the inflection point of the static magnetic scattering that increases with x [Figs. 4(b) and 4(d)]. The width of the peak at the FM position [Fig. 4(a)] determined by fitting a single Lorentzian (for the broad magnetic contribution) and a Gaussian [for the temperature independent weak nuclear contribution at (001)] gives a direct measure of the correlation length, ξ, obtained from the inverse of the half-width–half-maximum of the Lorentzian. As shown in Fig. 4(c), ξ increases abruptly but remains finite as the system enters the metallic phase due to the close relation between ferromagnetism and metallicity in this system. This indicates that the phase transition is percolative in nature involving FM clusters accompanied by macroscopic metallicity due to the double exchange mechanism. At the same time, we observed that for each concentration studied, ξ showed no temperature dependence in the ordered phase that contradicts recent small angle neutron scattering (SANS) data using powder samples [19]. This discrepancy might be due to the powder averaging artifact and/or the fact that SANS does not clearly discriminate elastic from inelastic contributions.

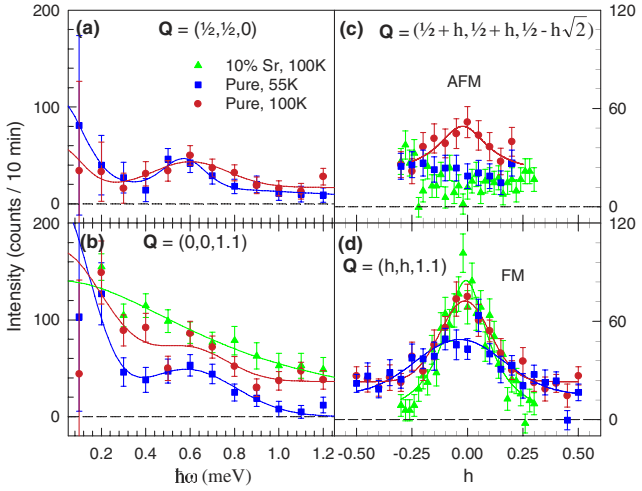

FIG. 3 (color online). Inelastic neutron scattering data obtained from the single crystals of $LaCoO_3$ and $La_{0.9}Sr_{0.1}CoO_3$ at SPINS. Constant-$\vec{Q}$ scans at (a) AFM $\vec{Q} = (\frac{1}{2}, \frac{1}{2}, 0)$ and (b) FM $Q = (001)$ wave vectors. Constant $\hbar\omega = 0.6$ meV scans centered at (c) AFM $Q = (\frac{1}{2}, \frac{1}{2}, \frac{1}{2})$ and (d) FM $Q = (001)$ points.

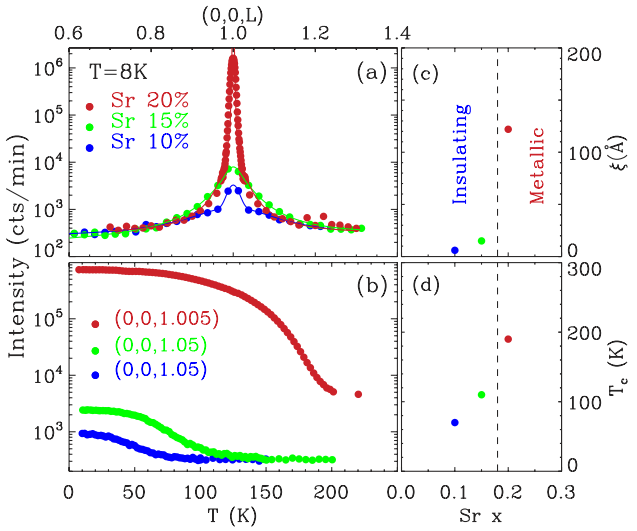

FIG. 4 (color online). (a) Elastic scan along $(0, 0, L)$ performed on single crystals of $La_{1-x}Sr_xCoO_3$ with $x = 0.1$, 0.15, and 0.2 at 8 K. The temperature dependence of (b) the elastic neutron scattering intensity, (c) of the ferromagnetic correlation length, ξ, and (d) of the spin freezing temperature, T_c.

Our neutron scattering results provide important information on key issues of the physics of $La_{1-x}Sr_xCoO_3$. In pure $LaCoO_3$, correlations between the thermally excited magnetic Co^{3+} ions have both FM and AFM characteristics. This can be explained by the Co ions in the intermediate $t_{2g}^5 e_g^1$, $S = 1$ state and with an orbital ordering that favors this state. The IS state is Jahn-Teller active as in the isostructural $LaMnO_3$ with $S = 2$, $t_{2g}^3 e_g^1$. In the latter, the degeneracy is broken through *static* Jahn-Teller orbital ordering leading to *A*-type AFM ordering consisting of FM interactions in the *ab* plane and AFM coupling between the planes coupled with a change in symmetry to orthorhombic [20]. The coexistence of *dynamic* FM and AFM correlations in $LaCoO_3$ suggests that orbital ordering analogous to the *A*-type ordering most likely occurs. We emphasize that the magnetic correlations are dynamic and short range with $\xi \approx 3.6$ Å that is close to the nearest neighbor Co-Co distance of $\sim$3.8 Å. This implies that the orbital correlations are also dynamic, and because of their short-range nature, they occur randomly in every direction. As a result, this generates dynamic FM and AFM correlations in every direction instead of the static and long-range *A*-type ordering of $LaMnO_3$. This can explain why magnetic scattering is observed at every integer and half-integer points. At the same time, the HS $S = 2$ state of the Co^{3+} ion is unlikely because only AFM correlations are expected between the $S = 2$ states [21]. The 0.6 meV mode is most likely due to transitions within the manifold of the thermally induced magnetic state [17], split in zero field due to the trigonal lattice distortion [22]. This is in good agreement with recent electron spin resonance studies that extracted from the field splitting of the resonance lines that $LaCoO_3$ has a spin triplet split by a uniaxial single-ion anisotropy, $D \approx 0.6$ meV [23].

With hole doping, short-range static FM correlations emerge at low temperatures. The FM correlations rapidly enhance as the system enters the metallic phase indicating that spins couple with charge via the DE mechanism [24]. Upon doping, magnetic Co^{4+} (t_{2g}^5, $S = 1/2$) ions form and induce the IS spin states of neighboring Co^{3+} ($t_{2g}^5 e_g^1$) ions [2], forming FM droplets. Within a droplet, charge hopping requires the e_g level for Co^{4+} to be empty and for Co^{3+} to be in the IS state and the two ions to be coupled ferromagnetically. Outside the droplet, spins couple dynamically and paramagnetically. When the droplet concentration gets large enough that connectivity is established between them, charge can then propagate over the lattice transforming the system to a metallic ferromagnet. In conclusion, our results provide indirect evidence in support of the thermally excited $S = 1$ IS state and dynamic orbital ordering in pure $LaCoO_3$. The addition of charges enhances the formation of nanoscale ferromagnetic droplets due to local DE interactions between the Co^{4+} and the IS spin state Co^{3+} ions.

Work at the University of Virginia is supported by the U.S. Department of Energy under Contract No. DE-FG02-01ER45927 and the U.S. DOC through NIST-70NANB5H1152, at the Los Alamos National Laboratory under Contract No. W-7405-Eng-36, and at the Argonne National Laboratory under Contract No. W-31-109-ENG-38. The use of the Neutron Scattering facilities at NIST was supported in part through NSF Grants No. DMR-9986442 and No. DMR-0086210.

*Corresponding author.
Electronic address: louca@virginia.edu

[1] P. M. Raccah and J. B. Goodenough, Phys. Rev. **155**, 932 (1967).
[2] D. Louca and J. L. Sarrao, Phys. Rev. Lett. **91**, 155501 (2003).
[3] A. Ishikawa, J. Nohara, and S. Sugai, Phys. Rev. Lett. **93**, 136401 (2004).
[4] Y. Tokura *et al.*, Phys. Rev. B **58**, R1699 (1998).
[5] G. Thornton, B. C. Tofield, and A. W. Hewat, J. Solid State Chem. **61**, 301 (1986).
[6] M. A. Korotin *et al.*, Phys. Rev. B **54**, 5309 (1996).
[7] V. G. Bhide *et al.*, Phys. Rev. B **12**, 2832 (1975); S. Yamaguchi, Y. Okimoto, and Y. Tokura, Phys. Rev. B **55**, R8666 (1997).
[8] T. Saitoh *et al.*, Phys. Rev. B **56**, 1290 (1997).
[9] D. Louca *et al.*, Phys. Rev. B **60**, R10378 (1999).
[10] K. Asai *et al.*, Phys. Rev. B **40**, 10 982 (1989).
[11] K. Asai *et al.*, Phys. Rev. B **50**, 3025 (1994).
[12] M. Itoh and I. Natori, J. Phys. Soc. Jpn. **64**, 970 (1995).
[13] P. L. Kuhns *et al.*, Phys. Rev. Lett. **91**, 127202 (2003).
[14] J. R. D. Copley and J. C. Cook, Chem. Phys. **292**, 477 (2003).
[15] S.-H. Lee *et al.*, Phys. Rev. B **56**, 8091 (1997).
[16] The 0.6 meV mode is of magnetic origin, as the intensity does not follow the Q^2 dependence of phonon modes and a field effect has been reported in Ref. [17].
[17] The 0.6 meV excitation was also observed recently in a powder by A. Podlesnyak *et al.*, cond-mat/0505344.
[18] L. P. Regnault *et al.*, Phys. Rev. B **38**, 4481 (1988).
[19] J. Wu *et al.*, Phys. Rev. Lett. **94**, 037201 (2005).
[20] T. Mizokawa and A. Fujimori, Phys. Rev. B **51**, R12880 (1995).
[21] R. H. Potze, G. A. Sawatsky, and M. Abbate, Phys. Rev. B **51**, 11 501 (1995).
[22] A. Abragam and B. Bleaney, *Electron Paramagnetic Resonance of Transition Ions* (Clarendon, Oxford, 1970), p. 19; also see R. J. Radwanski and Z. Ropka, Solid State Commun. **112**, 621 (1999).
[23] S. Noguchi *et al.*, Phys. Rev. B **66**, 094404 (2002).
[24] C. Zener, Phys. Rev. **81**, 440 (1951).
[25] J.-Q. Yan, J.-S. Zhou, and J. B. Goodenough, Phys. Rev. B **70**, 014402 (2004).